RESEARCH PAPER

A Facile Synthesis and Study of Photocatalytic Properties of Magnetic CaFe$_2$O$_4$-CeO$_2$ Nanocomposites Applicable for Separation of Toxic Azo Dyes

Fatemeh Saedi and Kambiz Hedayati *

Department of Science, Arak University of Technology, Arak, Iran

ARTICLE INFO

ABSTRACT

At the first step calcium ferrite nanostructures were synthesized via a facile precipitation method in the presence of green and compatible capping agent such as starch, poly vinyl pyrrolidone and glucose in solvent of water. Then cerium oxide nanoparticles and CaFe$_2$O$_4$-CeO$_2$ nanocomposites was made by a fast chemical procedure. The effect of temperature in nanoparticles and nanocomposites concentration and precipitating agent on the morphology and particle size of the products was investigated. The prepared products were characterized by X-ray diffraction (XRD), scanning electron microscopy (SEM), and Fourier transform infrared (FT-IR) spectroscopy. Also the crystalline size of nanoparticles was calculated by Debye-Scherrer formula. Vibrating sample magnetometer (VSM) shows the ferromagnetic property of the ferrite nanostructures. The photocatalytic behaviour of CaFe$_2$O$_4$-CeO$_2$ nanocomposites was evaluated using the degradation of three azo dyes (acid black, acid violet and acid blue) under ultraviolet light irradiation. The results introduce a nanocomposite with applicable magnetic and photocatalytic performance.

How to cite this article

INTRODUCTION

Aromatic compounds for examples azo dyes, pesticides and herbicides are widely used in industries and daily life, and are the principal pollutants and effluents discharge by companies. These organic pollutants distress the environment and human health due to their toxicity carcinogenicity and hazardous effect [1–3]. So the purification of these noxious organic compounds from the surrounding has received extreme research to preserve human health and environmental safety [4].

Conventional techniques such as precipitation, adsorption, reverse osmosis, oxidation, combustion, and biological methods were used so far for the purification of organic waste effluents.

But they lose their importance due to some drawbacks such as high cost, ineffectiveness, also they cannot destroy the organic dye molecules but just phase transfer the organic pollutions from water to another phase [5–9]. Photo-catalyst activity is an applicable method for purification of wastewater in the presence of semiconductor and it is an suitable option for the refining of organic pollutants [10,11]. Magnetic nanoparticles are great interest in science especially application in electronic inductors, transformers, also were used as a component of radar absorbing materials and etc [12,13].

CaFe$_2$O$_4$ easily forms and crystallizes in spinel structure and hence it would be interesting to study dielectrical and magnetic properties to assess its

* *Corresponding Author Email: K-hedayati@arakut.ac.ir*

suitability for various applications. In addition, it is important to synthesize CaFe$_2$O$_4$ compound because both the constituent metal cations Ca^{2+} & Fe^{3+} have zero crystal field stabilization energy for both tetrahedral and octahedral sites. CaFe$_2$O$_4$ crystallizes in orthorhombic structure with space group Pnma. Atomic arrangement is more compact in orthorhombic unit cell and hence the coordination around the cations was higher than that in the spinel [14-16]. For spinel ferrites synthesis many bottom up protocols such as co-precipitation, hydrothermal and sol-gel methods were popularly followed [14-17].

Cerium oxide one of the elements in lanthanide series is an excellent semiconducting material with a wide band gap which is familiar for its catalytic properties [18]. It is commonly used for enhancing efficiency or support in industrial catalytic processes due to its oxygen storage capacity [19].

Cerium has the capacity to switch over oxidation states (3+ and 4+) very easily and it is used in different usages for example catalytic converters, solid oxide fuel cells, oxygen buffers and corrosion protection [20,21]. The addition of metal oxide to CeO$_2$ significantly modifies catalyst activity, the oxygen storage capacity and surface area [22].

In this work cerium oxide and CaFe$_2$O$_4$-CeO$_2$ were made by a fast chemical procedure via low cost precursor materials. The photocatalytic efficiency of CaFe$_2$O$_4$-CeO$_2$ nanocomposites was evaluated using the decomposition of three azo dyes (acid black, acid violet and acid blue) under ultraviolet light irradiation. The results illustrate a nanocomposite with appropriate magnetic and photocatalytic application.

MATERIALS AND METHODS

Room temperature magnetic properties were investigated using vibrating sample magnetometer (VSM) device, made by Meghnatis Kavir Kashan Company (Iran) in an applied magnetic field sweeping between ±10000 Oe. XRD patterns were recorded by a Philips, X-ray diffractometer using Ni-filtered CuK$_\alpha$ radiation. SEM images were obtained using a KYKY instrument model EM-3200. Prior to taking images, the samples were coated by a very thin layer of Pt (using a BAL-TEC SCD 005 sputter coater) to make the sample surface conducting and prevent charge accumulation, and obtaining a better contrast. Fe(NO$_3$)$_3$ 9H$_2$O, Ca(NO$_3$)$_2$.4H$_2$O, Ce(SO$_4$)$_2$, starch, glucose, gelatin, salicylic acid, poly vinyl pyrrolidone and NaOH were purchased from Merck or Aldrich and all the chemicals were used as received without further purifications

Synthesis of CaFe$_2$O$_4$ nanoparticles

0.68 g of Fe(NO$_3$)$_3$ 9H$_2$O and 0.2 g of Ca(NO$_3$)$_2$ 4H$_2$O were dissolved in 200 ml of deionized water. 10 ml of NaOH solution (1M) was then slowly added to the solution until reaching pH to around 10. A brown precipitate was then centrifuged and rinsed with distilled water. Finally the obtained precipitate was calcinated at 80-500°C and its
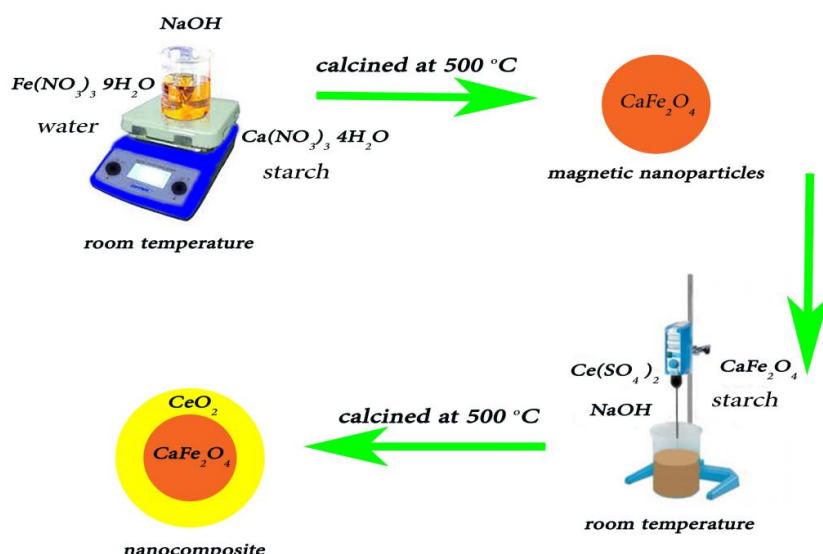

Fig. 1. Schematic of ferrite preparation nanocomposite.

colour goes from brown to black. Fig.1 shows the schematic diagram for experimental setup for nanoparticle and nanocomposite preparation used in the precipitation procedure. These conditions were chosen as a basic reaction in this work and effect of various parameters was investigated on the blank reaction.

Synthesis of CaFe$_2$O$_4$-CeO$_2$ nanocomposite

0.1 g of CaFe$_2$O$_4$ was dispersed in 200 ml of deionized water by ultrasonic waves (150 W, 8min). Then 0.4 g of Ce(SO$_4$)$_2$ was added. NaOH solution was slowly added to the aqueous solution until reaching pH to the 10 and was stirred for 30 minutes.

Photo-catalytic degradation process

0.1 g of catalyst was applied for degradation of 10 ml solution. The solution was mixed by a magnet stirrer for 1 hour in darkness to determine the adsorption of the dye by catalyst and better availability of the surface. The solution was irradiated by 8W UV lamp which was placed in a quartz pipe in the middle of reactor. It was turned on after 2 hour stirring the solution and sampling (about 10 ml) was done every 30 min. The samples were filtered, centrifuged and their concentration was determined by UV-Visible spectrometry.

RESULTS AND DISCUSSION

The crystallinity and composition of the CaFe$_2$O$_4$ nanoparticles was investigated. Fig. 2 shows XRD pattern of CaFe$_2$O$_4$ that reveals the typical diffraction pattern of pure orthorhombic phase (JCPDS No: 03-0825) with Pnma space group which is consistent with pure calcium ferrite. The crystallite phase of the CeO$_2$ nanoparticle was determined in Fig. 3. The XRD pattern of CeO$_2$ nanoparticles shows cubic phase (JCPDS No.: 34-0394) with Fm-3m space group which has agreement with pure CeO$_2$.

The composition of the CaFe$_2$O$_4$-CeO$_2$ nanocomposite was also investigated. Presence of both orthorhombic phase (JCPDS No.: 03-0825) and pure cubic phase (JCPDS No.: 34-0394) was confirmed and is illustrated in Fig. 4.

The crystalline sizes from Scherrer equation, D$_c$=0.9λ/βCosθ, was calculated, where β is the width of the observed diffraction peak at its half maximum intensity (FWHM), and λ is the X-ray wavelength (CuK$_\alpha$ radiation, equals to 0.154 nm). The average crystalline size for CaFe$_2$O$_4$, CeO$_2$ and CaFe$_2$O$_4$-CeO$_2$ nanoparticles were found to be about 19 , 21 and 29nm respectively.

Scanning electron microscopy was employed for estimation of morphology and particle size of the products. Fig. 5-a illustrate SEM images of the as-synthesized CaFe$_2$O$_4$ nanoparticles with glucose obtained at room temperature in 100 ml of solvent. The particle size and magnetic properties can be easily controlled by changing in precursors. The balance between nucleation and growth rates, determines final particle size so the morphology depends on the preparation conditions. The
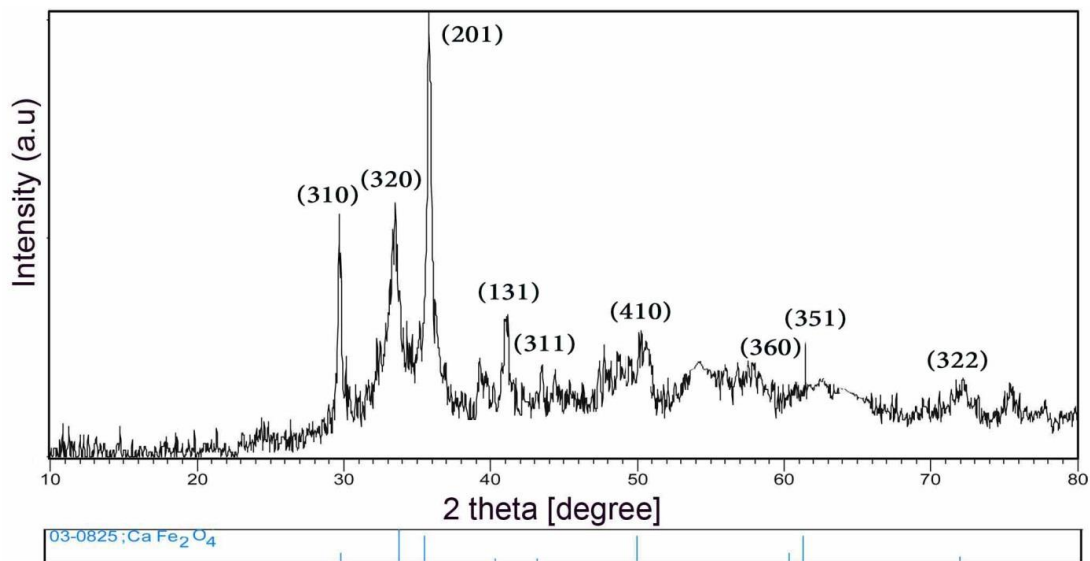

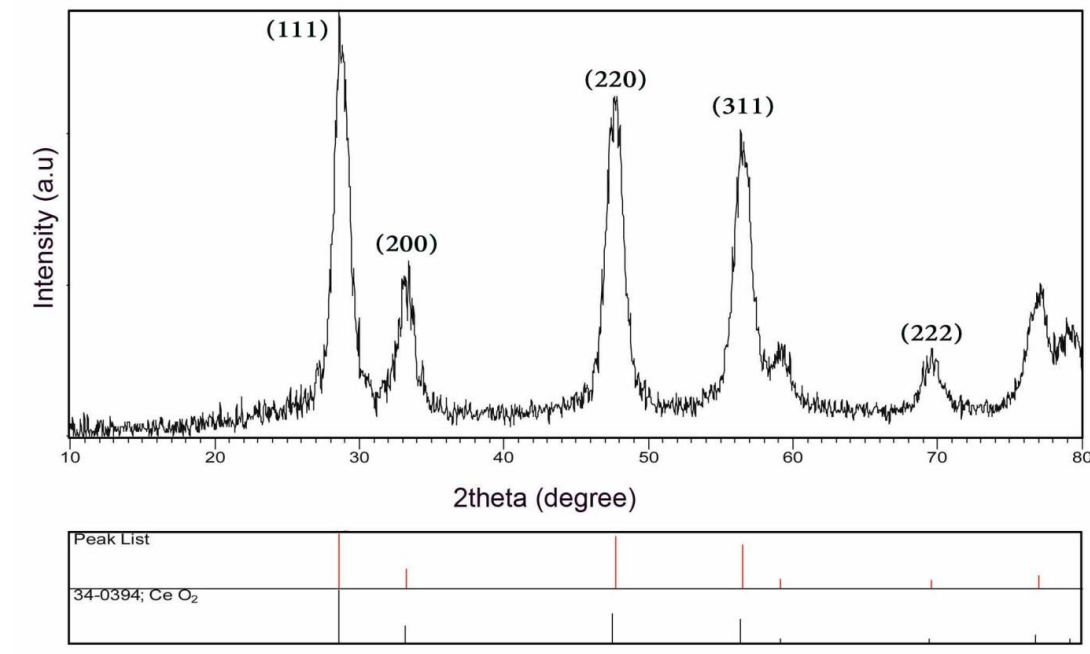
Fig. 2. XRD pattern of CaFe$_2$O$_4$ nanoparticles.

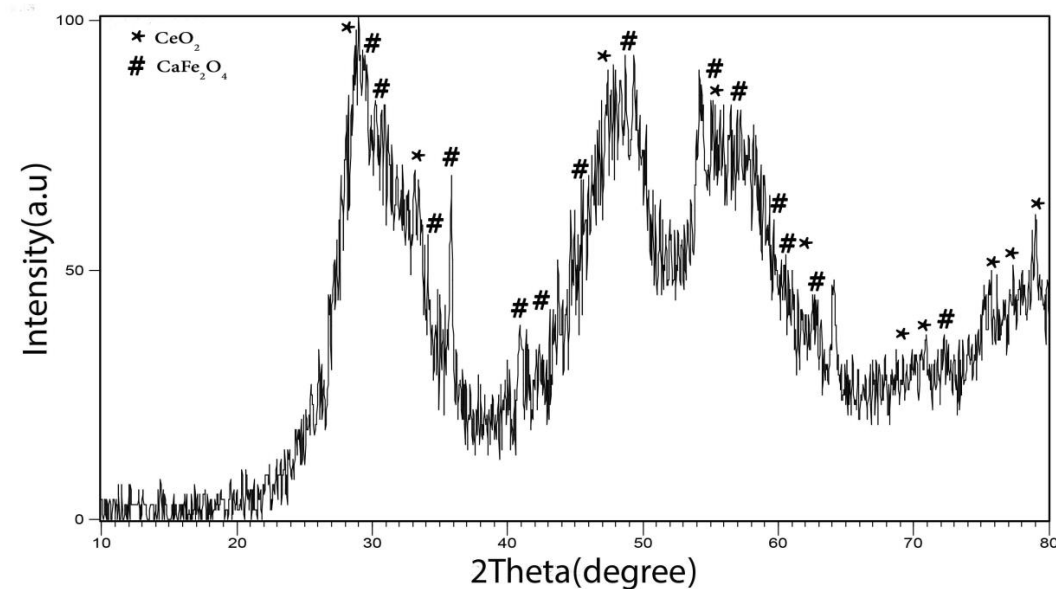Fig. 3. XRD pattern of CeO$_2$ nanoparticles.

Fig. 4. XRD pattern of CaFe$_2$O$_4$-CeO$_2$ nanocomposite.

average particle size is about 58 nm.

Fig. 5-b show SEM images of the calcium ferrite nanoparticles prepared with starch surfactant. According to scanning electron microscopy images the average particle size is found to be around 54 nm.

SEM images of calcium ferrite nanoparticles with poly vinyl pyrrolidone as neutral capping agent are illustrated in Fig. 5-c. Images approve the mean particle size is about 40 nm.

Fig. 5-d show SEM images of the calcium ferrite nanoparticles obtained applying gelatin surfactant
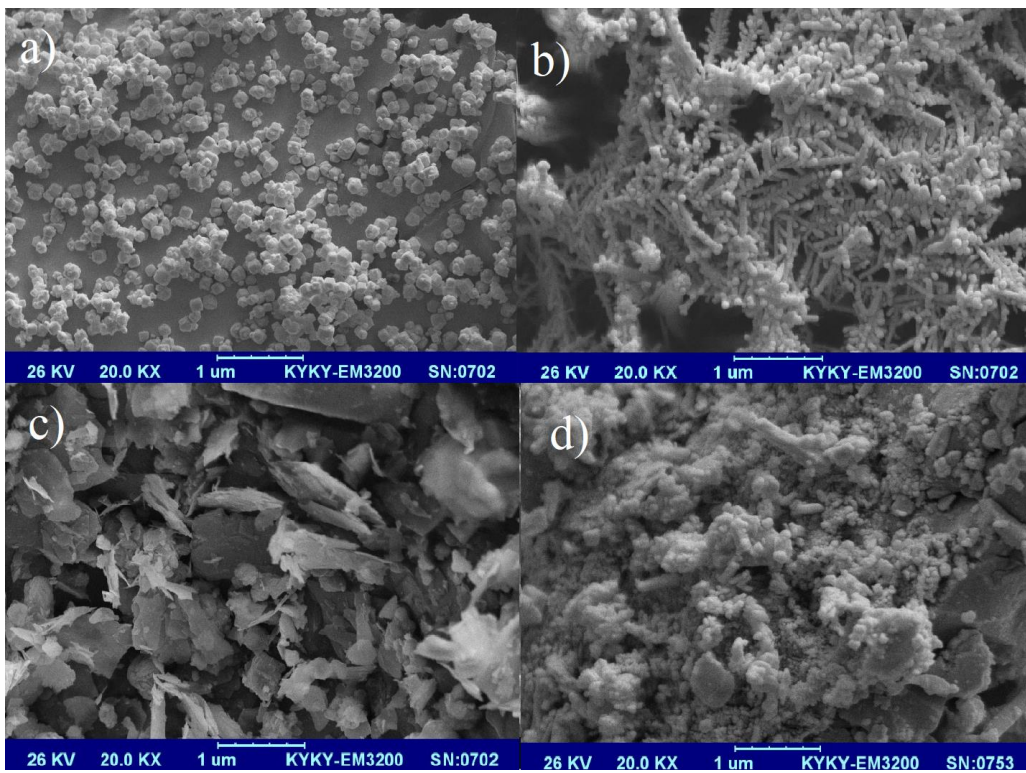
Fig. 5. SEM images of calcium ferrite nanoparticles with a) glucose, b) starch, c) poly vinyl pyrrolidone and d) gelatin.
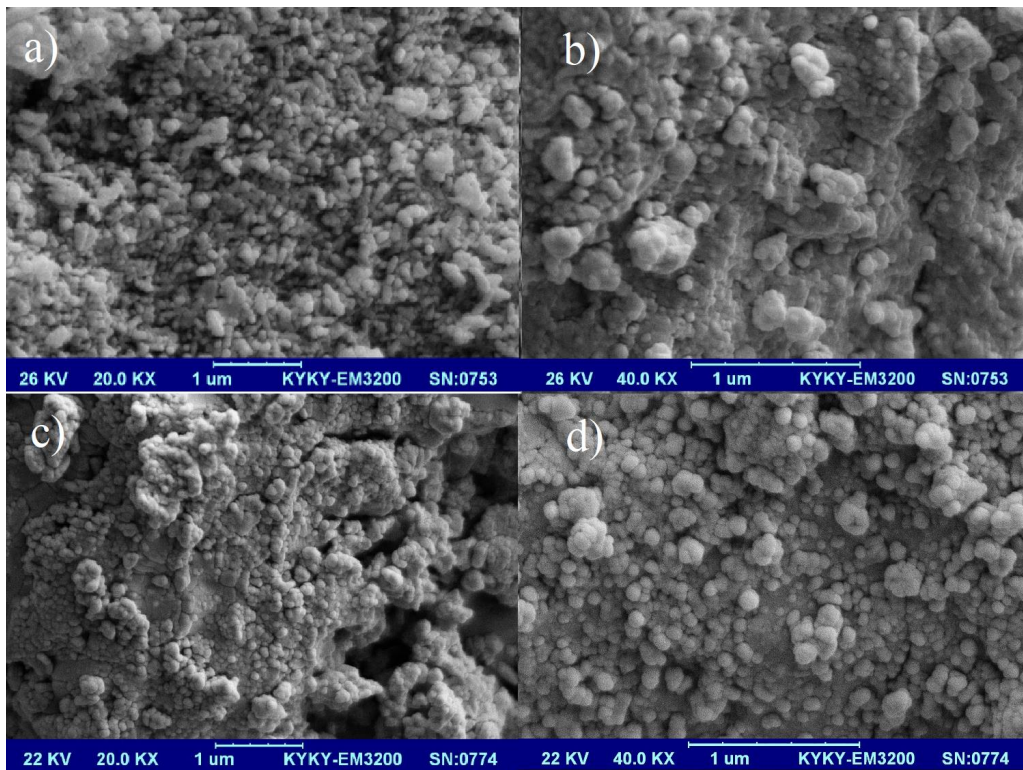

Fig. 6. SEM images of calcium ferrite nanoparticles a) with salicylic acid calcined at 500 °C, b) by applying KOH, c) by using starch and d) prepared at 200 ml of water.
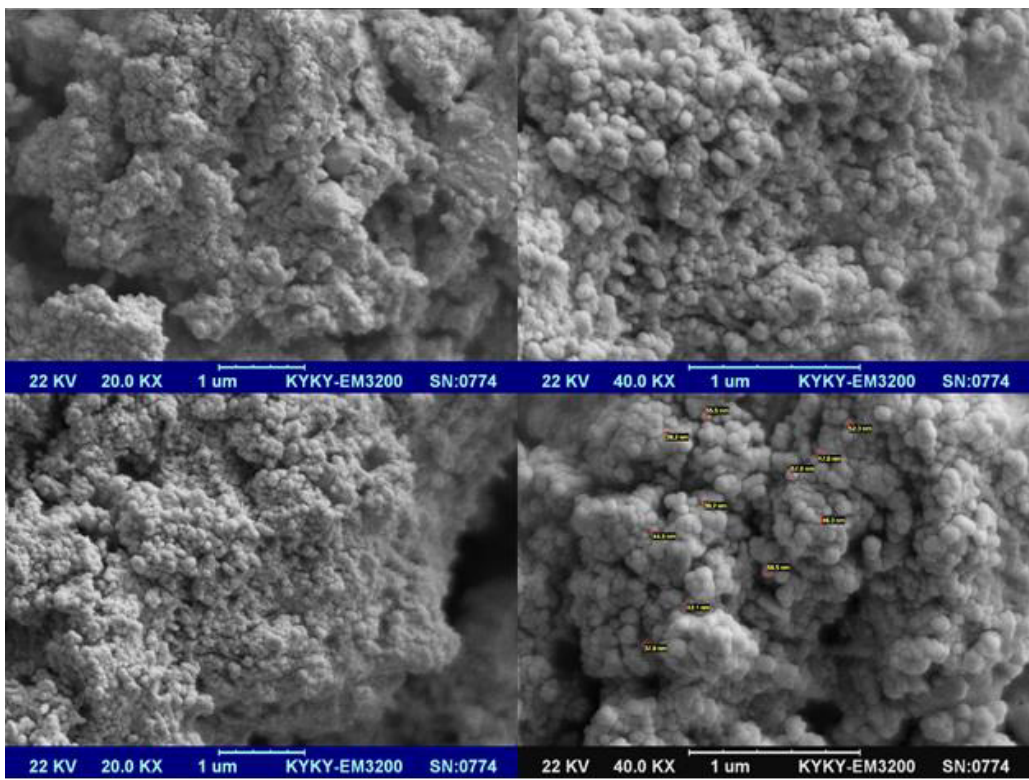
Fig. 7. SEM images of calcium ferrite nanoparticles via hydrothermal method
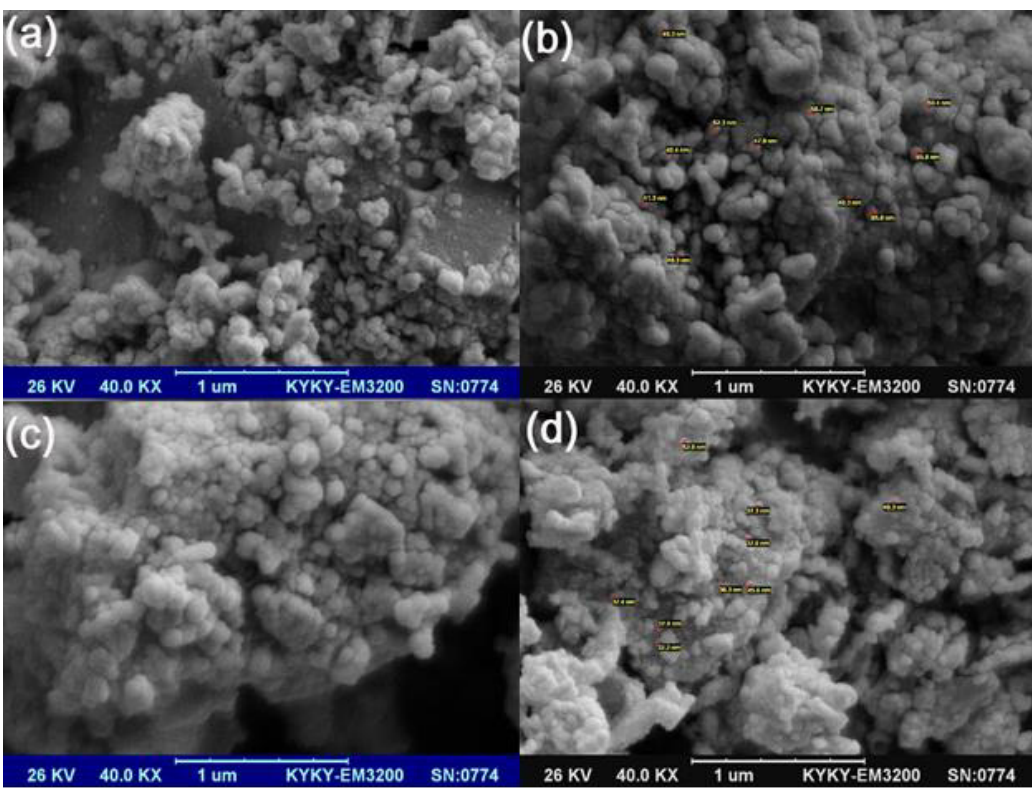

Fig. 8. (a,b) SEM images of the room temperature prepared CeO_2 (c,d) SEM images of the CeO_2 that calcined at 500 °C

calcinated at 500 °C. According to scanning electron microscopy images the average particle size is found to be around 41 nm.

Fig. 6-a show SEM images of the calcium ferrite nanoparticles obtained in the presence of salicylic acid surfactant calcinated at 500 °C. Related to SEM images the mediocre particle size is about 36nm.

The effect of another precipitating agent on the morphology and size of the ferrites was examined Fig. 6-b show SEM images of the calcium ferrite obtained using potassium hydroxide as a precipitating agent. Diameter of the magnetic products is less than 51 nm.

The effect of both temperature and capping agent on the size of the products was also examined. Fig. 6-c illustrate SEM images of calcium ferrite nanoparticles with starch coating at calcination temperature about 500° C. The mediocre size was estimated to be around 45 nm. The results confirmed that all synthesized nanostructures were formed from nanoparticles with average diameter size less than 100 nm. Fig. 6-d illustrates the effect of lower concentration on the calcium ferrite with starch coating, the

obtained product in 200ml (instead of 100 ml) of solvent approve formation of nanoparticles. The average particle size of diluted product is about 45 nm.

Fig. 7 shows the calcium ferrite images prepared by the hydrothermal method. Scanning electron microscopy images verify dimensions are less than 47 nm.

SEM images of the cerium dioxide nanoparticles prepared at room temperature without calcination are shown in Figs.8-a-b. The average particle size is about 49 nm. And SEM images of the CeO$_2$ nanoparticles that calcined at 500°C are illustrated in the Figs.8-c-d. Average dimensions of both products are calculated to be around 41 nm.

Fig. 9. illustrate SEM images of the as-synthesized CaFe$_2$O$_4$-CeO$_2$ obtained at 80°C in 200ml of solvent. That result confirms nanocomposites with average size around 45 nm were obtained.

Fig. 10-a shows the FT-IR spectrum of the as-prepared CaFe$_2$O$_4$ nanoparticles at 500 °C, the absorptions band at 314, 442 and 557cm^{-1} are assigned to the stretching mode of Fe-O and Ca-O bonds. The spectrum exhibits broad
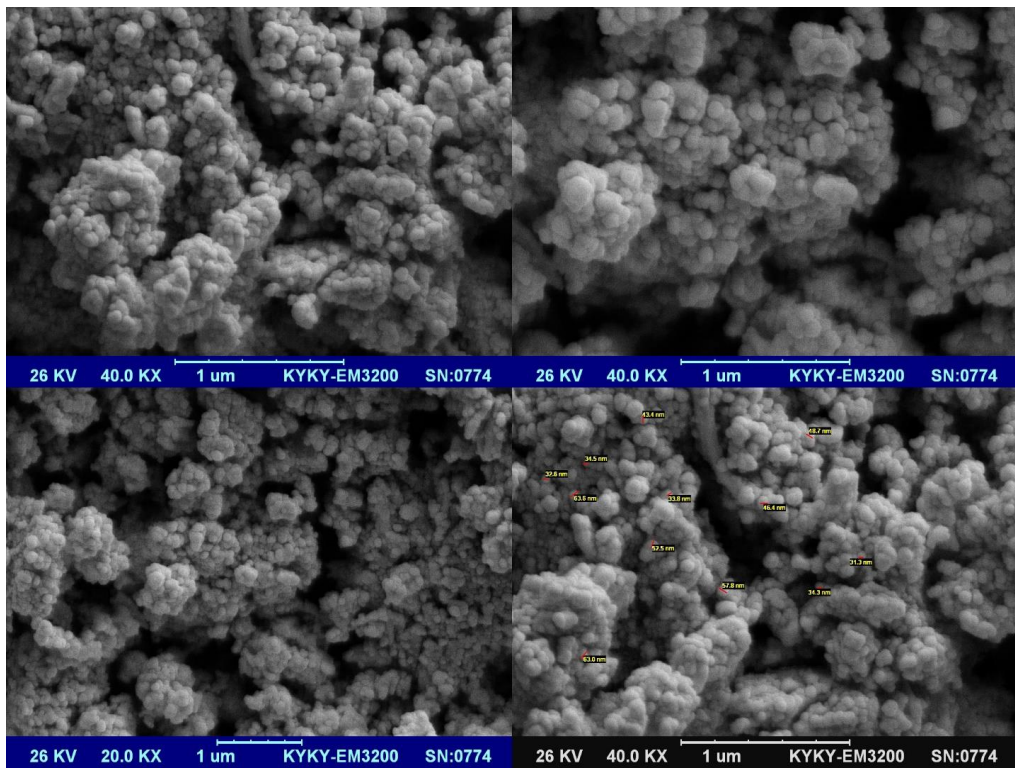

Fig. 9. SEM images of CaFe$_2$O$_4$-CeO$_2$ nanocomposite

absorption peak around 3423cm^{-1}, corresponding to the stretching mode of O-H group of hydroxyl group and the weak band near 1467 cm^{-1} is assigned to H–O–H bending vibration mode due to the adsorption of moisture on the surface of nanoparticles.

FT-IR spectrum of the CeO$_2$ nanoparticle at 500 °C is shown in Fig. 10-b. The very intense bands between 1384 and 1459 cm^{-1} are attributed to Ce–O bonds. The spectrum exhibits broad absorption peak around 3435 cm^{-1}, corresponding to the stretching mode of hydroxyl group which adsorbed on the surface of nanostructures.

Fig. 10-c illustrates the FT-IR spectrum of the as-prepared CaFe$_2$O$_4$-CeO$_2$ nanocomposites at 500 °C. The hydrothermally prepared CeO$_2$ nanoparticles contain small amounts of carbonate ions and the absorption peak was aroused at 1372cm^{-1}. Broad
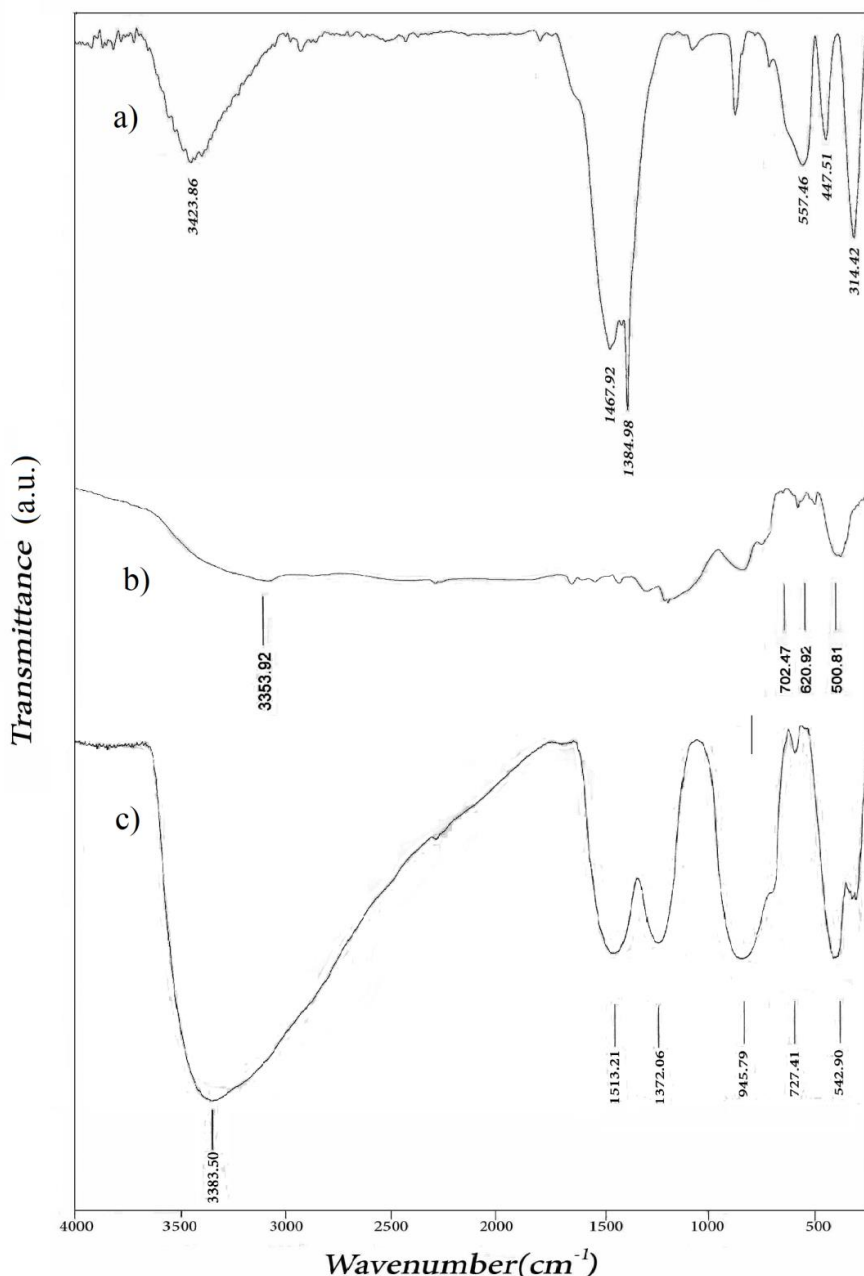

Fig. 10. FT-IR spectrum of a) CaFe$_2$O$_4$ nanoparticles, b) CeO$_2$ nanoparticles and c) CaFe$_2$O$_4$-CeO$_2$ nanocomposite.

absorption around 3383 cm^{-1} is corresponding to the O-H group. All absorptions band at 727 and 542 cm^{-1} are assigned to the stretching mode of Ca-O and Ce-O bonds.

Magnetic property of the room prepared magnetic sample was studied using VSM instrument, and the obtained is shown in Fig. 11. The result indicates that, the sample

exhibit ferromagnetic property. A saturation magnetization around 0.88 emu/g, and coercivity about 41.5 Oe have been achieved.

Fig. 12 shows magnetization curve of CaFe$_2$O$_4$ that calcined at 500 °C. Also exhibits also ferromagnetic behaviour with a coercivity of about 35 Oe and saturation magnetization of 2.5 emu/g.

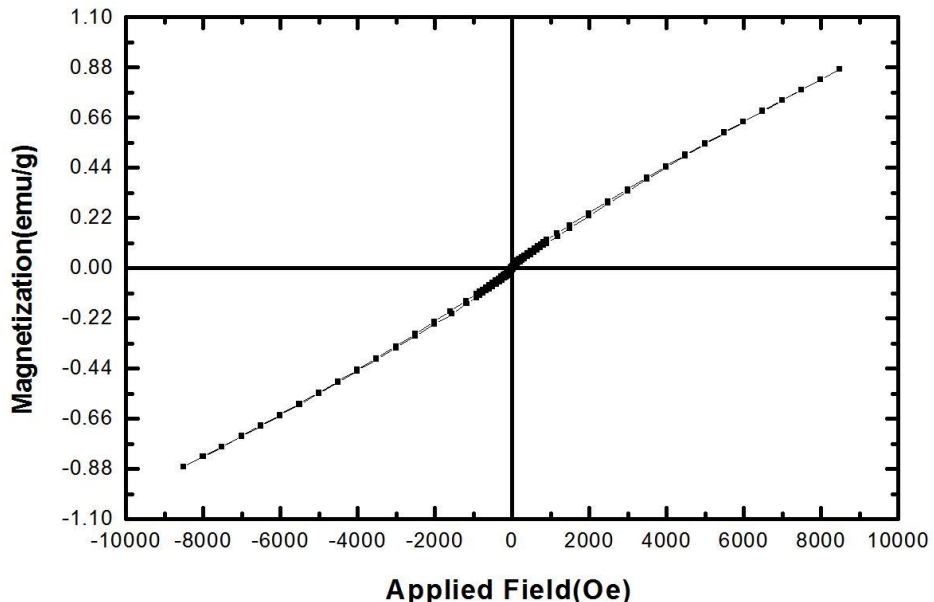Fig. 13 illustrates magnetization curve of

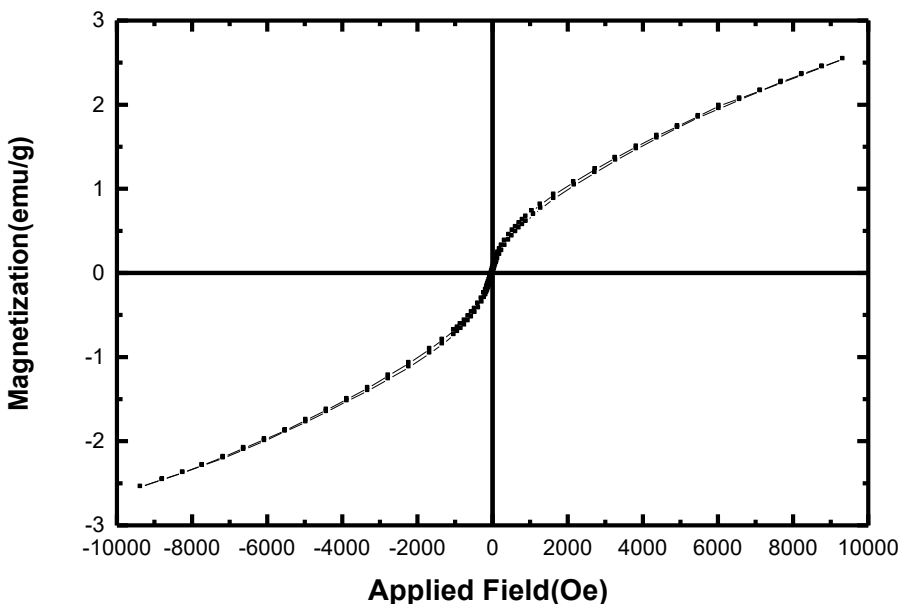Fig. 11. VSM curve of room- temperature prepared calcium ferrite nanoparticles

Fig. 12. VSM curve of calcium ferrite nanoparticles calcined at 500 °C
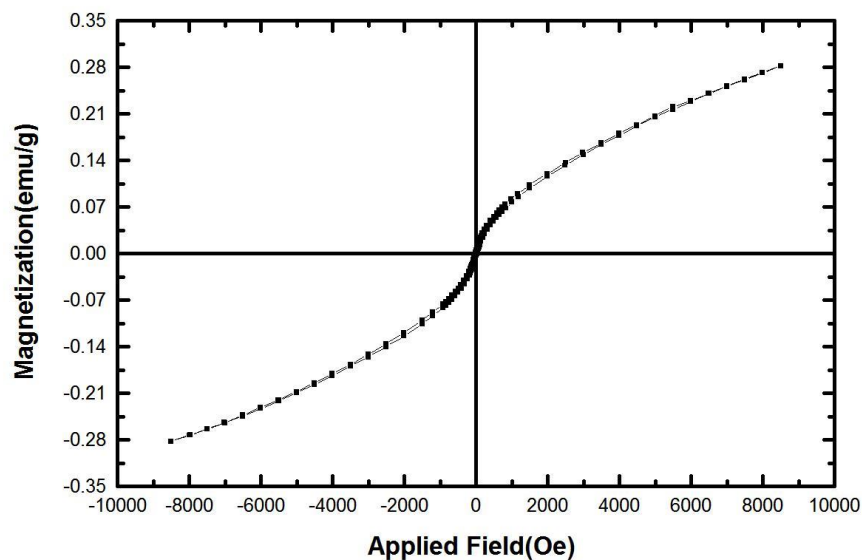
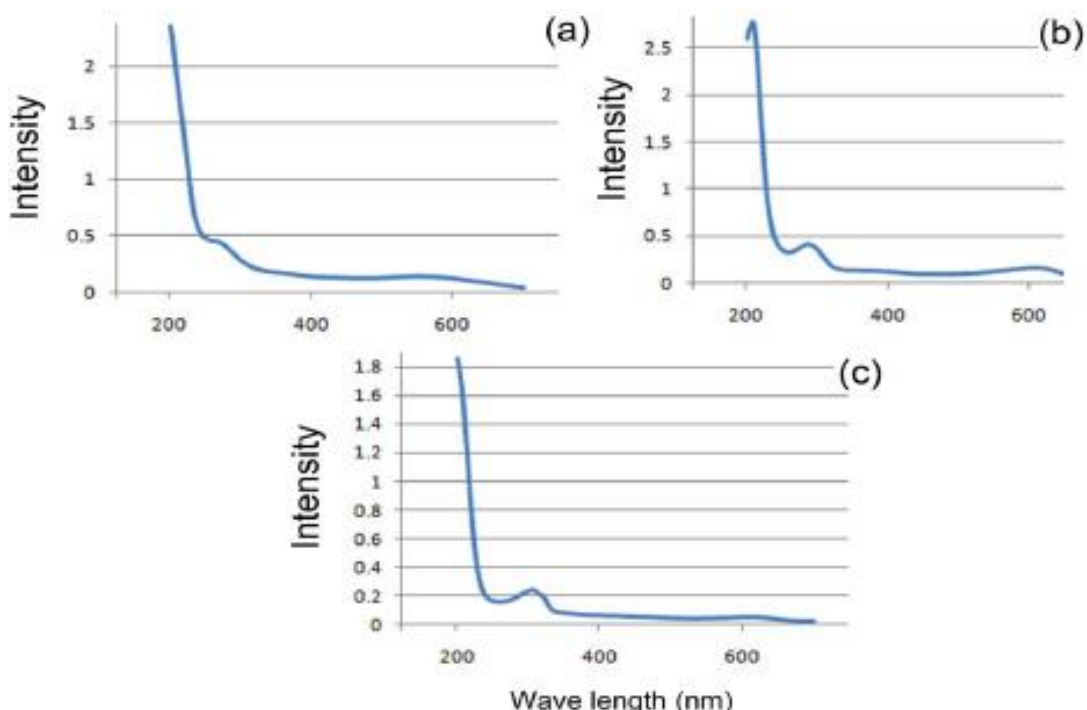Fig. 13. VSM curve of CaFe$_2$O$_4$-CeO$_2$ nanocomposite

Fig. 14. UV-Vis absorption (a) acid black (b) acid blue (c) acid violet

CaFe$_2$O$_4$-CeO$_2$ that also exhibits also ferromagnetic behaviour with a coercivity of about 23 Oe and saturation magnetization of 0.28 emu/g.

The magnetic property of the prepared nanocomposites is an essential characteristic of a heterogeneous nanocomposite since materials with this magnetic behaviour have low tendency in inter-particles agglomeration caused by dipole-dipole interaction in comparison with ferromagnetic nanocomposites.

Acid black, acid violet and acid blue as typical organic pollutants were employed as targets
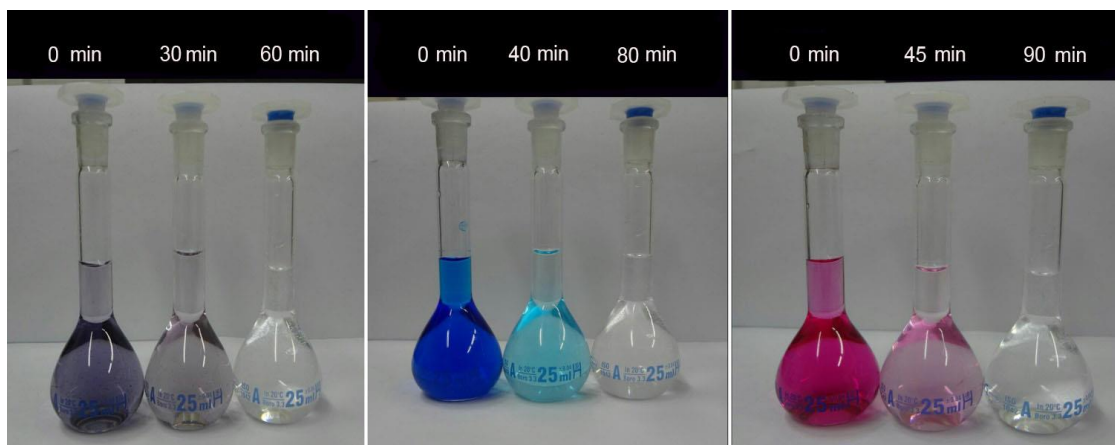
Fig. 15. Photo-degradation of (a) acid black 1 (b) acid blue 92 and (c) acid violet 43

because of the relative stability of their molecular structure. UV-Vis absorption of these azo dyes under ultra violet in the presence of CaFe$_2$O$_4$-CeO$_2$ are shown in Fig 14. The as-prepared nanocomposite has the potential to be applied to improve environmental problems associated with organic and toxic water pollutants.

Maximum absorption peaks (λmax) of organic dyes that were used for degradation under UV light are prepared from UV-vis absorption spectra and were confirmed by scientific literature. Acid black, acid violet and acid blue were degraded 60, 80 and 90min respectively by CaFe$_2$O$_4$-CeO$_2$ nanocomposite. As time increase dyes are adsorbed on the nanoparticles catalyst, until the absorption peaks (λmax) of acid black, and acid blue decrease and vanish around 90 min (Fig. 14). The dyes concentration decreased rapidly with increasing UV-irradiation time organic dyes decompose to carbon dioxide, water and other less toxic or nontoxic residuals The changes in the concentration of dye are illustrated in Fig.15 [23-25].

CONCLUSIONS

In conclusion, synthesis, characterization, and photocatalytic activity of CaFe$_2$O$_4$, CeO$_2$ nanoparticles and CaFe$_2$O$_4$-CeO$_2$ nanocomposite were reported. VSM hysteresis loop confirmed that ferrite nanoparticles and nanocomposite exhibit ferromagnetic behaviour. The photocatalytic behaviour of CaFe$_2$O$_4$-CeO$_2$ nanocomposite was investigated by the degradation of acid black, acid blue, and acid violet azo dyes under UV light irradiation. The results indicate that precipitation method is a suitable method for preparation of CaFe$_2$O$_4$-CeO$_2$ nanocomposites as a candidate for photocatalytic applications to digration azo dyes.

CONFLICT OF INTEREST

The authors declare that there are no conflicts of interest regarding the publication of this manuscript.

REFERENCES

1. Hedayati K, Azarakhsh S, Saffari J, Ghanbari D. Photo catalyst CoFe$_2$O$_4$–CdS nanocomposites for degradation of toxic dyes: investigation of coercivity and magnetization, Journal of Materials Science: Materials in Electronics. 2016; 27 (8): 8758-8770.

2. Lahijani L, Hedayati K, Goodarzi M. Magnetic PbFe$_{12}$O$_{19}$-TiO$_2$ nanocomposites and their photocatalytic performance in the removal of toxic pollutants. Main group metal chemistry. 2018; 41 (3-4): 53-62.

3. Ravelli D, Dondi D, Fagnoni M, Albini A. Photocatalysis. A multi-faceted concept for green chemistry Chem Soc Rev 2009; 38: 1999-2011.

4. Malato S, Fernández-Ibanez P, Maldonado M I, Blanco J, Gernjak W, Decontamination and Disinfection of Water by Solar Photocatalysis: Recent Overview and Trends. Catalysis Today. 2009; 147(1):1-59.

5. Yang L Y, Dong S Y, Sun J H, Feng J L, Wu Q H, Sun S P. Microwave-assisted preparation, characterization and photocatalytic properties of a dumbbell-shaped ZnO photocatalyst. J Hazardous Mater. 2010; 179: 438-443.

6. Hedayati K, Joulaei M, Ghanbari D. Auto combustion synthesis using grapefruit extract: photocatalyst and magnetic MgFe$_2$O$_4$-PbS nanocomposites. J Nanostruct. 2020; 10(1): 127-131.

7. Song X C, Zheng Y F, Yang E, Liu G, Zhang Y, Chen H F, Zhang Y Y. Photocatalytic activities of Cd-doped ZnWO$_4$ nanorods prepared by a hydrothermal process. J Hazardous Mater 2010; 179: 1122-1127.

8. Ebrahimi Z, Hedayati K, Ghanbari D. Preparation of hard magnetic BaFe$_{12}$O$_{19}$–TiO$_2$ nanocomposites: applicable for photo-degradation of toxic pollutants. Journal of Materials Science: Materials in Electronics. 2017; 28(18): 13956-

13969.

9. Sun J H, Dong S Y, Wang Y K, Sun S P. Preparation and photocatalytic property of a novel dumbbell-shaped ZnO microcrystal photocatalyst. J Hazardous Mater 2009; 172(2-3): 1520-1526.

10. Qiu R, Zhang D, Mo Y, Song L, Brewer E, Huang X, Xiong Y. Photocatalytic activity of polymer-modified ZnO under visible light irradiation. J Hazardous Mater 2008; 156: 80-85.

11. Hedayati K. Synthesis and characterization of nickel zinc ferrite nanoparticles. J Nanostruct. 2015; 5(1): 13-16.

12. Raj K, Moskowitz R, Casciari R. Advances in ferrofluid technology. J Magn Magn Mater. 1995; 149(1-2): 174-180.

13. Suryanarayana C, Mechanical alloying and milling. Progress in Material Science. 2001; 46(1-2): 1 – 184.

14. Manohar A, Krishnamoorthi C , Structural, optical, dielectric and magnetic properties of CaFe2O4 nanocrystals prepared by solvothermal reflux method. J Alloys Compd, 2017; 722: 818-827.

15. Wang Z, Schiferl D, Zhao Y, High pressure Raman spectroscopy of spinel-type ferrite $ZnFe_2O_4$, J Phys Chem Solids. 2003; 64(12): 2517-2523.

16. Hedayati K, Kord M, Goodarzi M, Ghanbari D, Gharigh S. Photo-catalyst and magnetic nanocomposites: hydrothermal preparation of core–shell $Fe_3O_4@PbS$ for photo-degradation of toxic dyes. J Mater Sci: Mater Electron. 2017; 28(2): 1577–1589.

17. Hedayati K, Behesht-Ara Z, Ghanbari D. Preparation and characterization of various morphologies of $SrFe_{12}O_{19}$ nano-structures: investigation of magnetization and coercivity. J Mater Sci: Mater Electron. 2017; 28(1): 1-9.

18. Trovarelli A, Zamar F, Llorca J, de Leitenburg C, Dolcetti G, Kiss J T, Nanophase Fluorite-Structured $CeO_2–ZrO_2$ Catalysts Prepared by High-Energy Mechanical Milling. J Catalysis. 1997; 169(2): 490-502.

19. Celerier S, Laberty-Robert C, Long J W, Pettigrew K A, Stroud R M, D.R.. Rolison D R, F. Ansart F, Stevens P, Synthesis of $La_{9.33}Si_6O26$ Pore–Solid Nanoarchitectures via Epoxide-Driven Sol–Gel Chemistry Adv Materials. 1997; 18(5): 615-618.

20. Creus J, Brezault F, Rebere C, Gadouleau M. Synthesis and characterisation of thin cerium oxide coatings elaborated by cathodic electrolytic deposition on steel substrate. Surf Coat Tech. 2006; 200(14-15): 4636 – 4645.

21. Hedayati K, Goodarzi M, Kord M. Green and facile synthesis of Fe3O4-PbS magnetic nanocomposites applicable for the degradation of toxic organic dyes. Main group metal chemistry. 2016; 39(5-6): 183-194.

22. Masoumi S, Nabiyouni G, Ghanbari D. Photo-degradation of azo dyes: photo catalyst and magnetic investigation of $CuFe_2O_4–TiO_2$ nanoparticles and nanocomposites. J Mater Sci: Mater Electron 2016; 27 (9): 9962-9975.

23. Hassanpour M, Salavati-Niasari M, Tafreshi SA, Safardoust-Hojaghan H, Hassanpour F. Synthesis, characterization and antibacterial activities of Ni/ZnO nanocomposites using bis (salicylaldehyde) complex precursor. J Alloys Compd. 2019;788:383-390.

24. Ghanbari D, Sharifi S, Naraghi A, Nabiyouni G. Photo-degradation of azo-dyes by applicable magnetic zeolite Y–Silver–$CoFe_2O_4$ nanocomposites. J Mater Sci: Mater Electron. 2016; 27(5): 5315-5323.

25. Yousefi S R, Ghanbari D, Salavati-Niasari M, Hassanpour M, Photo-degradation of organic dyes: simple chemical synthesis of $Ni(OH)_2$ nanoparticles, $Ni/Ni(OH)_2$ and Ni/NiO magnetic nanocomposites. J Mater Sci: Mater Electron. 2016; 27(2): 1244-1253.